Chinese Chemical Letters 34 (2023) 108000

Contents lists available at ScienceDirect

Chinese Chemical Letters

journal homepage: www.elsevier.com/locate/cclet

Advances in catalytic elimination of atmospheric pollutants by two-dimensional transition metal oxides

Rong Li [a,b,c], Yongfang Rao [d], Yu Huang [a,b,*]

[a] Key Laboratory of Aerosol Chemistry and Physics, State Key Laboratory of Loess and Quaternary Geology (SKLLQG), Institute of Earth Environment, Chinese Academy of Sciences, Xi'an 710061, China
[b] Center of Excellence in Quaternary Science and Global Change, Chinese Academy of Sciences, Xi'an 710061, China
[c] University of Chinese Academy of Sciences, Beijing 100049, China
[d] Department of Environmental Science and Engineering, Xi'an Jiaotong University, Xi'an 710049, China

ARTICLE INFO

Article history:
Received 6 September 2022
Revised 8 November 2022
Accepted 9 November 2022
Available online 13 November 2022

Keywords:
Two-dimensional structure
Transition metal oxides
Atmospheric pollutants
Catalytic elimination
Preparation method

ABSTRACT

Atmospheric pollutants can deteriorate air quality and put human health at risk. There is a growing need for green, economical, and efficient technologies, among which catalytic elimination technology is the most promising, to remove atmospheric pollutants. Two-dimensional transition metal oxides (2D TMOs) have recently become attractive catalysts due to their highly exposed active sites, excellent reactant transport properties, and extraordinary catalytic performance. This review systematically summarizes the top-down and bottom-up preparation methods of 2D TMOs and focuses on the specific applications of 2D TMOs in the catalytic elimination of atmospheric inorganic pollutants and volatile organic pollutants. The development of 2D TMOs in the catalytic elimination of atmospheric pollutants is prospected. This review is expected to provide design insights into efficient 2D TMOs to remove atmospheric pollutants.

1. Introduction

The rapid development of industrialization and urbanization has led to serious atmospheric pollution, which mainly comes from industry, transportation, agriculture, and domestic emissions [1–3]. Atmospheric pollutants include particulate matter and gaseous pollutants, the latter can be divided into inorganic gaseous pollutants (such as CO, NO_x, SO_2, and O_3) and volatile organic pollutants (VOCs, such as methane, toluene, formaldehyde, acetone, trichloroethylene). These pollutants can directly harm human health [4,5] and damage the atmospheric environment (causing acid rain, photochemical smog, and haze) [6–8]. Among numerous control methods, catalytic elimination with the superiority of high efficiency, low energy consumption, strong stability, and wide applicability is considered to be the most promising treatment technology. In a typical catalytic elimination process, atmospheric pollutants pass over the catalyst fixed in the reactor. By means of additional energy input (such as light and heating), catalytic elimination utilizes the oxidation or reduction of atmospheric pollutants on catalyst surface to transform them into harmless substances [9–11]. The key to catalytic technology is developing catalysts with high activity, stability, and selectivity. Transition metal oxides (TMOs) favored by researchers have been extensively applied to the catalytic elimination of atmospheric pollutants due to their low cost, good catalytic activity, strong stability, and easy modification [12–14].

At present, TMOs have been modified by various methods, such as morphology regulation [15], compounding [16,17], doping [18], defect engineering [19], phase engineering [20], and loading noble metal [21] to promote the generation of active sites. However, the catalytic elimination of atmospheric pollutants occurs on the catalyst surface, which leaves the internal active sites of conventional bulk TMOs invalid. Fortunately, two-dimensional (2D) structures can be constructed to effectively increase the proportion of catalyst surface structures [22], thereby significantly promoting the utilization of active sites and improves the catalytic elimination performance. 2D nanomaterials possess sheet-like nanostructures, whose lateral dimensions typically larger than 100 nm or up to several μm. Their thicknesses range from single to multiple unit cells (usually less than 5 nm) [23]. Constructing an ultrathin 2D nanosheet structure can greatly increase the specific surface area and promote the generation of low-coordination atoms on the surface of TMOs, thereby introducing a large number of dangling bonds and promoting the quantity and exposure of active sites [24,25]. Furthermore, to maintain structural stability, the surface lattice of 2D

* Corresponding author at: Key Laboratory of Aerosol Chemistry and Physics, State Key Laboratory of Loess and Quaternary Geology (SKLLQG), Institute of Earth Environment, Chinese Academy of Sciences, Xi'an 710061, China.
E-mail address: huangyu@ieecas.cn (Y. Huang).

https://doi.org/10.1016/j.cclet.2022.108000
1001-8417/

TMOs is easier to distort and reconfigure, leading to changes in electronic states and significantly improves the activity of lattice oxygen and metal sites, which facilitates rapid chemisorption of reactants and abundant formation of reactive species [26,27]. In addition, the confinement effect of the 2D structure accelerates the transport of electrons and reactants [28–30].

According to the characteristics of the layered structure, 2D TMOs can be divided into layered TMOs and non-layered TMOs [31]. The interlayers of layered TMOs, including TiO_2, V_2O_5, MnO_2, NbO_x, MoO_3, RuO_2, TaO_3, and WO_3 are connected by weak van der Waals forces, forming a stacked layered structure [32]. Generally, the host phase of layered TMO nanosheets is negatively charged, so the interlayer gaps can stabilize the layered structure through accommodating foreign cations (such as Na^+, K^+, Rb^+, and Cs^+) [33–35]. Non-layered 2D TMOs, such as Co_3O_4, ZnO_2, CeO_2, Fe_2O_3, SnO_2, and NiO, inherently have ordered crystal structures with all atoms connected by strong chemical bonds in three dimensions [36]. In contrast, layered 2D TMOs more easily achieve a single atomic layer structure, providing full exposure of active sites. Although non-layered 2D TMOs have difficulty constructing single-layer nanosheets, their lattice edges can exhibit abundant lattice distortion and electronic state reorganization [37], inducing the formation of highly active and energetic surfaces.

Several reviews have introduced the applications of 2D TMOs in sensor [38,39], energy storage [40,41], antimicrobial [42,43], and cancer therapy [44], but systematic discussion on the research of 2D TMOs in the purification of atmospheric pollutants is lacking. Therefore, this review details the preparation methods of different types of 2D TMOs and summarizes their applications in the catalytic elimination of atmospheric pollutants. In addition, the structure-activity relationship of different 2D TMOs has been emphasized. Finally, this review prospects the development of 2D TMOs in the catalytic elimination of atmospheric pollutants.

2. Preparation method

Although 2D TMOs possess many advantages in the catalytic elimination of atmospheric pollutants, their controllable and large-scale preparation still faces huge challenges. The preparation methods of 2D TMOs can be divided into two categories: top-down and bottom-up. The top-down preparation relies on the exfoliation of bulk precursors of TMOs to obtain ultrathin nanosheets and is usually only applicable to layered TMOs [45]. The bottom-up preparation relies on specific synthesis conditions to restrict the growth of metal oxides or steer their precursors to grow only in two-dimensional plane directions [46]. The latter can be used to prepare both layered TMOs and non-layered TMOs. The summary of preparation method for 2D TMOs is shown in Table S1 (Supporting information).

2.1. Top-down preparation

Energy can be applied to the bulk precursors of layered TMOs by physical, chemical or electrochemical methods to destroy the van der Waals forces between layers to obtain many monolayers or few layers of 2D TMOs. These methods are easy to handle, through which high yield and high crystallinity of 2D TMOs can be obtained. However, top-down preparation is not suitable for non-layered 2D TMOs and the size of the obtained nanosheets is not controllable [28]. Top-down preparation mainly includes mechanical exfoliation, soft chemical exfoliation, and electrochemical exfoliation.

Mechanical exfoliation is a method that bulk metal oxide precursors are sonicated in a specific liquid. Ultrasound can generate abundant cavitation bubbles around the bulk material. The mechanical energy generated during the collapse of the bubbles

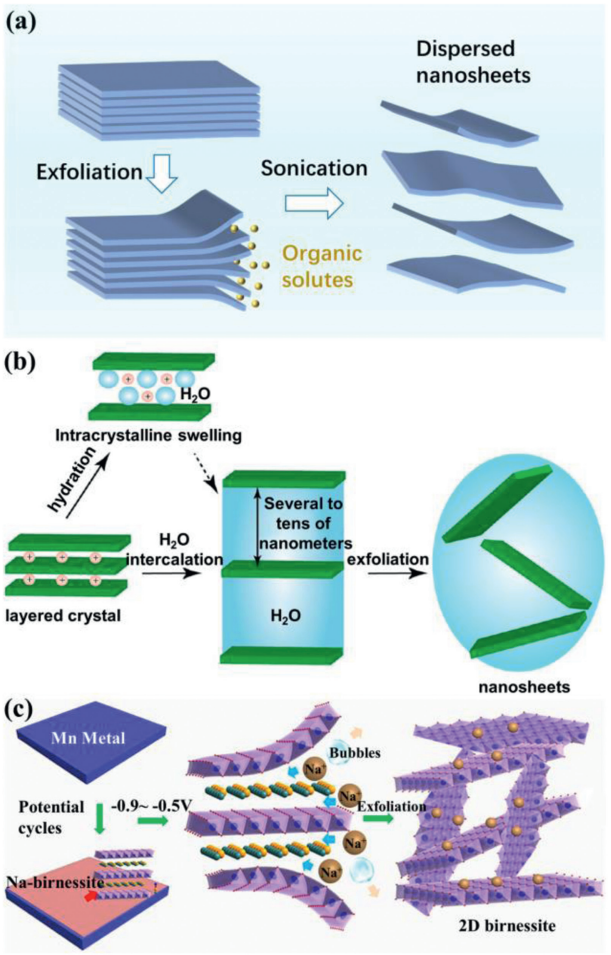

Fig. 1. Schematic illustration of (a) mechanical exfoliation in aqueous solutions of organic solutes, (b) the swelling and soft exfoliation process. Reproduced with permission [54]. Copyright 2014, American Chemical Society. (c) The fabrication of 2D birnessite through an electrochemical potential-cycle exfoliation process. Reproduced with permission [59]. Copyright 2021, Elsevier.

can destroy the interlayer van der Waals force of layered TMOs under nonuniform pressure, thus promoting interlayer separation [47]. After sonicating for a certain time, a dispersion containing 2D nanosheets can be obtained. Solvent choice is the key factor in ultrasonic exfoliation. Similar to the procedure in Fig. 1a, Alsaif *et al.* [48] investigated the differences among *N*-methyl-2-pyrrolidone (NMP), acetonitrile, methanol, ethanol and isopropanol (IPA) aqueous solutions in the exfoliation of MoO_3 powder by the sunlight-assisted ultrasound method, and found that the minimum average thickness of the obtained MoO_3 nanoflakes was 4 nm (IPA aqueous solution). Similarly, Hanlon *et al.* [49] preferred IPA, in which MoO_3 powder was ultrasonically exfoliated. They found that only nanosheets with lengths below 200–300 nm could maintain stable dispersion. In addition, the smaller the lateral dimension of the nanosheets, the thinner the nanosheets (the thinnest thickness is a few atomic layers). Solutions containing surfactants or polymers as well as organic solvents are also widely used. The high surface energy between the layered TMOs and the solvent can effectively reduce the exfoliation energy of the nanosheets from the bulk precursor, thereby improving the exfoliation efficiency [50]. Besides, the repulsive force between the surfactant (or polymer) and the 2D nanosheets can prevent the aggregation of the exfoliated ultrathin nanosheets [51]. Furthermore, the temperature control of the solvent is critical for the exfoliation of layered TMOs [47]. However, simple mechanical exfoliation is suitable for a few TMOs because

the host layer of most layered metal oxides is negatively charged and the interlayer interaction is strong.

Given that it is infeasible for ultrasound to exfoliate the strongly negatively charged layered TMOs, soft chemical exfoliation is applied to overcome the interlayer electrostatic resistance based on ion intercalation and exchange [52]. Since most negatively charged layered TMOs contain exchangeable alkali metal cations to balance the charge, ion intercalation or exchange is employed to assist exfoliation [53]. Generally, the interlayer cations can be exchanged for H^+ by acid solution treatment. Subsequently, H^+ cations can be replaced by larger organic ammonium ions (such as methylammonium, propylammonium, tetrabutylammonium hydroxide, and tetramethylammonium hydroxide) in alkaline solution, causing the TMOs to swell [54]. Meanwhile, a large number of H_2O molecules are introduced, thereby reducing the interlayer van der Waals force and greatly extending the interlayer distance [40]. Finally, relying on ultrasonic-assisted mechanical exfoliation, the swollen TMOs can be easily exfoliated into ultrathin nanosheets (Fig. 1b). Some ultrathin nanosheets such as $Ti_{0.87}O_2^{0.52-}$, $MnO_2^{0.4-}$, and $Ca_2Nb_3O_{10}^-$ are prepared by the above soft chemical exfoliation steps, and their thicknesses are ~1.2, ~0.8, and ~2.3 nm, respectively [55]. In addition, interlayer cations can also be substituted by polar organic solvents. Lee *et al.* [56] used HCl to treat bulk layered TMOs such as $A_{x/4}Ti_{1-x}O_2$, A_xMnO_2, and A_xRuO_2 (A = alkali metal), and the products were added to various polar solvents (formamide, dimethyl sulfoxide, ethanol, methanol, IPA, 1-butanol and acetone) followed by sonication at room temperature to obtain 2D TMOs. Soft chemical exfoliation can realize the batch preparation of 2D TMOs, but it is difficult to control the nanosheet thickness and requires complicated preparation steps and high costs.

In view of the slow exchange rate of interlayer cations and solution cations in the soft chemical exfoliation method, electrochemical exfoliation in a three-electrode electrolytic cell has recently been developed, which greatly reduces the exfoliation time. When the voltage is applied to the working electrode and the reference electrode, the ions in the electrolyte solution rapidly migrate to the interlayers of the bulk TMOs to expand the interlayer structure, leading to the delamination of TMOs [57]. In addition, the electrolyte can provide surface tension to prevent the agglomeration of the exfoliated 2D nanosheets [58]. As shown in Fig. 1c, Yang *et al.* [59] proposed a one-pot electrochemical potential cyclic exfoliation method. Through a procedure of anodic dissolution, cathodic deposit, and cathodic exfoliation, 2D layered birnessite with interlayer Na, K, and Li cations were synthesized by using bulk manganese metal sheets as precursors and aqueous NaOH, KOH and LiOH as electrolytes.

2.2. Bottom-up preparation

For the bottom-up method, atoms or molecules in solution or gas phase can be assembled and grown into 2D ultrathin nanosheets under certain conditions [60]. Therefore, this method is appropriate for the synthesis of 2D layered and non-layered TMOs. Bottom-up preparation is characterized by strong controllability, high yield, uniform nanosheets, and no limitation. However, it is difficult to obtain nanosheets with atomic layer thickness and requires long preparation time and possibly introduces toxic reagents [38]. Bottom-up methods mainly include chemical vapor deposition (CVD), solvothermal method, self-assembly method, template method, and molten salt method.

In CVD method, the precursors of TMOs evaporate and decompose under heating, and then the decomposed products migrate through the gas phase and deposit onto cooler substrates, where they finally nucleate and grow into 2D nanosheets [61]. Rasoul *et al.* [62] synthesized K-doped 2D MnO_2 in a real-time optical observation CVD chamber. In this study, KI and MnO_2 powders were ground into fine powder. Subsequently, the c-plane sapphire substrate was heated to 640 °C, and 2D K-MnO_2 with a lateral dimension of 100 μm and a thickness of approximately 0.7 nm was obtained after 5 min. Li *et al.* [63] utilized a high temperature CVD method to dissolve rare earth metal oxide (REO) powder into molten Au on Mo foil. After cooling, REO was uniformly dispersed and nucleated on the Au surface. This method also used NH_4X ($X^- = Cl^-$, Br^-, I^-) to control the crystal facet exposure (Fig. 2a), resulting in 2D REO nanosheets with different thicknesses (1–5 nm). The superiority of CVD is that the thickness, crystallinity, and exposed crystal planes of 2D nanosheets are highly controllable. However, the high cost, uneven distribution of nanosheets, and low yield limit its application in air pollutant purification.

The solvothermal method is currently the most widely used method for preparing 2D TMOs. Generally, solvothermal reactions are carried out in a solution environment at high temperature and pressure. In a closed reactor, metal precursors are dissolved in water or organic solvents, where structure-directing agents, including cetyl trimethyl methylammonium bromide (CTAB) [64], polyvinylpyrrolidone (PVP) [65], polyethylene glycol (PEG) [66], polyethylene oxide-polypropylene oxide-polyethylene oxide (P123) [67], and sodium lauryl sulfate (SDS) [68] can be optionally added. After reaction for a certain time, 2D TMOs or their precursors are obtained, and the latter can be transformed into 2D TMOs through a topological transformation reaction [69]. Gao *et al.* [70] reported a typical solvothermal preparation of 2D TMOs: cobalt acetylacetonate and CTAB were added to ethylene glycol/H_2O solvent and stirred well. Subsequently, the reaction solution was transferred to a Teflon-lined autoclave and heated at 180 °C for 20 h. Finally, the precursor was acquired by washing, centrifugation and drying. Then they are pyrolyzed into single-layer Co_3O_4 nanosheets with a thickness of 0.84 nm (Fig. 2b). Wang *et al.* [71] synthesized $Cu(OH)_2$, the precursor of CuO, by a surfactant-free hydrothermal method, which was carried out by heating an aqueous solution containing $Cu(SO_4)_2$, KOH and ammonia in a closed reactor at 80 °C. After the pyrolysis of $Cu(OH)_2$, CuO nanosheets with thicknesses of 3-4 nm were acquired. Zhao *et al.* [72] poured nickel foam carriers into a $KMnO_4$ solution. After solvothermal reaction at 180 °C for 3 h, ultrathin δ-MnO_2 nanosheet arrays with only two atomic layers (1.4 nm) were grown on the surface of nickel foam. In general, solvothermal methods which are cost effective and simple, are suitable for any TMOs and generate the 2D TMOs with high purity and good dispersion. However, solvothermal method is time-consuming and generates a large amount of waste liquid.

The self-assembly method depends on the interaction (including van der Waals force, hydrophilicity and hydrophobicity, electrostatic interaction) between the reactants in solvent to assemble the dispersed precursor ions or molecules into a regularly arranged structure (Fig. 2c) [73]. Zhang *et al.* [74] reported a general strategy for the controllable synthesis of 2D TMOs through modulating the phase transition induced by micelles at low temperature. After adding P123 to the aqueous solution of metal salt, the spherical micelles were transformed into lamellar micelles with the temperature increased from 0 to 50 °C and the addition of ammonia or ethylenediamine. After rapid hydrolysis, a metal hydroxide was formed, which can be calcined to obtain 2D TMOs (including Mn_3O_4, Fe_2O_3, Co_3O_4, NiO, CuO, ZnO, SnO_2 and Sb_2O_3). In addition, the auxiliaries introduced by self-assembly can be applied for an *in situ* doping of nonmetallic elements. Xing *et al.* [75] prepared a $Co(C_3H_5O_2N)_2$ complex through the self-assembly of alanine in ethanol/H_2O solution with cobalt acetate and alanine continually mixed, which underwent dehydration condensation to form twisted and stable peptide structures. The planar coordination structure of Co^{2+} facilitated the arrangement of the complex into a 2D structure, which self-assembled through weak interactions to form cross-network nanostructures. Finally, N-doped 2D

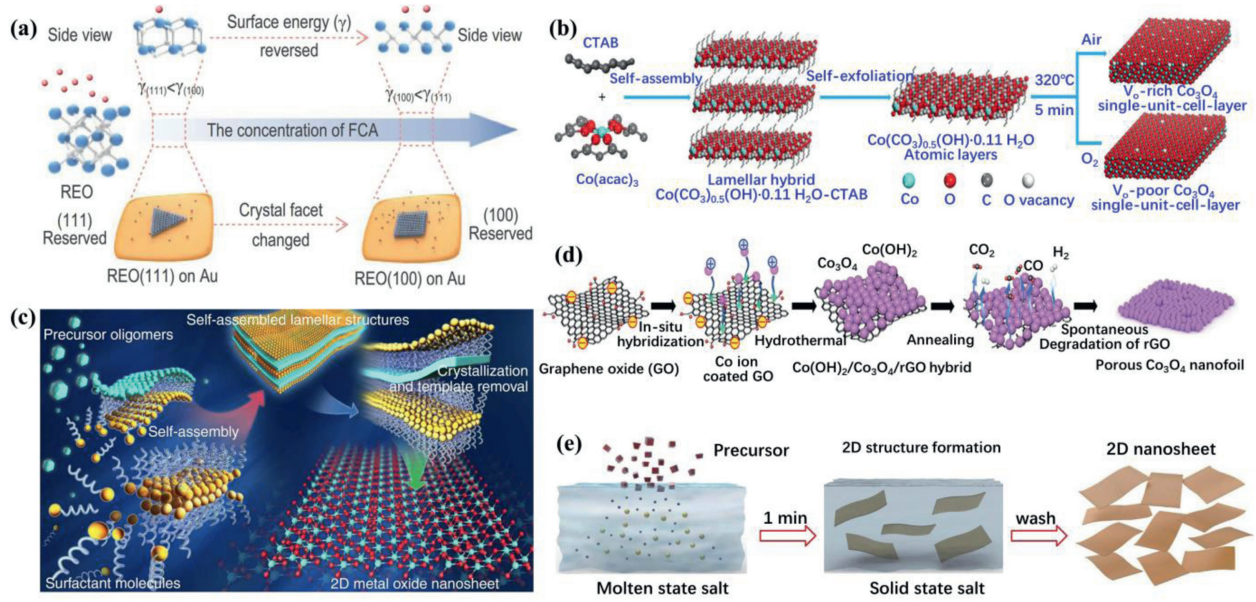

Fig. 2. Schematic illustration of (a) the high temperature CVD method for 2D REO assisted by a face control strategy. Copied with permission [63]. Copyright 2021, Oxford University Press. (b) The solvothermal method for the formation of Co_3O_4 single-unit-cell layer. Reproduced with permission [70]. Copyright 2017, Nature. (c) Self-assembly of 2D metal oxide nanosheets. Copied with permission [73]. Copyright 2014, Nature. (d) GO-templated method for the preparation of porous 2D Co_3O_4. Reproduced with permission [80]. Copyright 2014, Wiley Publishing Group. (e) Molten salt method synthesis of 2D oxides. Reproduced with permission [84]. Copyright 2017, Nature.

Co_3O_4 with rich defects was obtained after annealing in air. Similar to solvothermal methods, the self-assembly method is suitable for most TMOs and has the advantages of simplicity and high efficiency. However, the addition of a large amount of organic additives is bound to increase the cost, and this method is not expert at controlling the thickness precisely.

The template method utilizes the existing stable nanomaterials in the liquid phase as the substrate so that the growth of TMOs or their precursors are curbed in 2D space. The target product with a 2D structure is obtained after the template is removed [76]. Templates can be divided into three categories: soft templates, hard templates and salt templates. Soft templates are mainly surfactants, which are widely applied in hydrothermal method and self-assembly method. Most hard template methods use 2D graphene oxide (GO), whose surface has abundant oxygen functional groups and large π bonds, favorable for the adsorption of metal cations through electrostatic adsorption in the liquid phase [77,78]. Lei *et al.* [79] thoroughly mixed GO nanosheets and metal nitrate precursors in ethanol. Then, the reaction solution was dried, and the acquired powder was ground to obtain GO-metal composites, which were calcined in air to prepare a series of 2D TMOs. Among them, the thinnest 2D CeO_2 nanosheets (3.7 nm) display large lateral dimensions, abundant surface Ce^{3+} species and oxygen vacancies. Eom *et al.* [80] mixed aqueous dispersed GO with cobalt ion solution. This system was then hydrothermally reacted at 180 °C to synthesize a mixture of Co_3O_4 and $Co(OH)_2$, which was further annealed at 600 °C in air to obtain 2D porous Co_3O_4 (Fig. 2d). The simple GO template method is versatile and suitable for the generation of large-scale 2D metal oxide nanosheets. However, high cost and low yield of this method cannot be ignored. For the salt template method, the matching between the surface lattices of water-soluble salt crystals and oxide lattices allows water-soluble salt crystals to serve as growth substrates for 2D TMOs [36,81]. Li *et al.* [82] reported a method to support 2D mixed-phase CoO/Co_3O_4 nanosheets on graphene surfaces using a water-soluble salt template strategy. First, NaCl, cobalt acetate, and GO were mixed in aqueous solution with stirring. Then, liquid nitrogen quenching was used to promote the formation of wrinkles on the GO surface to adsorb nucleating ions. Meanwhile, the gradual sublimation of H_2O resulted in the recrystallization of NaCl, whose outer layer was wrapped by cobalt precursor. After calcination and washing to remove NaCl, GO-supported 2D CoO/Co_3O_4 with a thickness of 3 nm graphene was obtained. Although salt template method can prepare 2D nanosheets with large lateral sizes and has the advantages of high yield, low cost and easy recovery, this method is only applicable to the preparation of a few metal oxides.

In the abovementioned bottom-up method, the diffusion length of reactants is long, and the diffusion speed is slow, which makes the reaction time-consuming. The molten salt method uses metal ion precursors, additives and molten salts as raw materials. When all of them are melted, most of the ionic/covalent bonds are destroyed so that metal ions are rapidly transported and recrystallized to grow products. Finally, the molten salts are removed by washing [83]. Molten salt method shows the advantages of extremely short reaction time, simple operation, and large-scale preparation, but only a few TMOs are currently applicable. Hu *et al.* [84] reported a rapid and large-scale production by molten salt method, which mixed manganese sulfate with $NaNO_3$ or KNO_3 molten salt, and ammonium tungstate hydrate with $LiNO_3$ or $NaNO_3$. Cationically intercalated 2D manganese oxides and tungsten oxides with thicknesses of 1–4 nm were acquired by heating these mixtures at 300–400 °C for only 1 min (Fig. 2e). In addition, the use of low-melting-point salts with 2D structures as templates is a further development of molten salt method. $CoCl_2{\cdot}6H_2O$ is a typical 2D compound with a low melting point (86 °C). Based on this, Gu *et al.* [85] proposed a general, fast (5 min) and low-temperature (approximately 100 °C) $CoCl_2$ molten salt method for the large-scale preparation of a series of ultrathin (2–7 nm) 2D TMOs including MoO_3, SnO_2, SiO_2 and $ZnCo_2O_4$, with large horizontal sizes. When $CoCl_2{\cdot}6H_2O$ and metal chlorides were fully mixed and heated to 100 °C and maintained for 5 min, the metal chlorides were hydrolyzed to produce the corresponding TMOs. After the reaction solution cooled down, $CoCl_2$ could still form $CoCl_2{\cdot}6H_2O$, thus confining the generated TMOs in the interlayer of $CoCl_2{\cdot}6H_2O$. Fi-

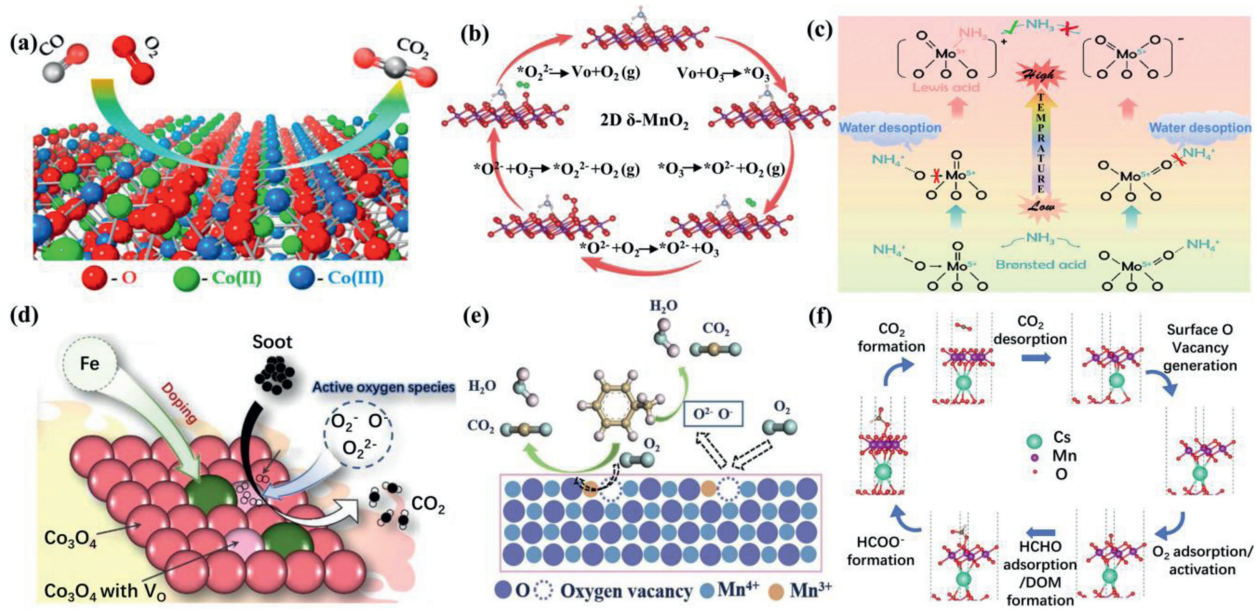

Fig. 3. Schematic diagram of (a) CO oxidation on Co_3O_4 (112) facet. Copied with permission [90]. Copyright 2019, American Chemical Society. (b) Ozone decomposition pathway for 2D δ-MnO_2. Reproduced with permission [98]. Copyright 2021, Royal Society of Chemistry. (c) Influence of catalyst structure and acid site conversion on NH_3-SCR reaction pathway. Reproduced with permission [105]. Copyright 2022, Elsevier. (d) Catalytic combustion mechanism of soot on Fe-doped Co_3O_4. Reproduced with permission [110]. Copyright 2022, Elsevier. (e) Reaction pathway of toluene on MnO_2 catalyst with oxygen vacancy. Copied with permission [124]. Copyright 2018, Royal Society of Chemistry. (f) Reaction cycle for HCHO oxidation on Cs-intercalated MnO_2. Reproduced with permission [132]. Copyright 2020, American Chemical Society.

nally, 2D TMOs can be obtained by simple water washing and centrifugation.

3. Application in the elimination of atmospheric pollutants

Given that 2D TMOs combine the advantages of 2D structures and oxides, they have abundant and highly exposed active sites, as well as excellent redox properties. Therefore, 2D TMOs have been widely applied in the catalytic oxidation or catalytic reduction of atmospheric pollutants. In this section, we systematically summarize the 2D TMOs-based catalytic technologies for removing atmospheric inorganic pollutants (including CO, O_3, NO_x, and soot) and volatile organic pollutants.

3.1. CO

Carbon monoxide (CO) is a high content of gaseous pollutants in the atmosphere. CO mainly derives from the incomplete combustion process of fossil fuels and solid wastes. Vehicle exhaust is the largest combustion source [86]. Due to the affinity of CO toward human hemoglobin, even a small amount of CO can seriously endanger human health and even be fatal [87]. TMOs have excellent oxygen cycling ability and can catalyze the oxidation of CO into CO_2 down to room temperature through lattice oxygen or surface-absorbed reactive oxygen species (ROS) [88]. Co_3O_4 with a spinel structure is considered to be the most active TMO at low temperature for CO oxidation, but its activity highly depends on environmental humidity. Competitively adsorbed H_2O can bind surface O to convert CO into stable formate/carbonate [89]. Exposure of highly active crystal facets to specific contaminants can lower the energy barrier of the reaction and improve the selectivity of active sites [18]. Based on this, Cai *et al.* [90] prepared 2D Co_3O_4-assembled nanoflower catalysts with an average thickness of 2.4 nm by solvothermal and topological transformation methods. This catalyst exposed up to 70% of the (112) facet which had an open surface structure with abundant surface defects (grain boundaries, steps, and atomic vacancies), leading to the increased formation of unsaturated bonds. In a dry environment, 2D Co_3O_4 maintained 100% CO conversion efficiency at 22–200 °C (Fig. 3a). When the reaction temperature was higher than 150 °C, this activity still remained stable under saturated water vapor (Fig. S1a in Supporting information). Jin *et al.* [91] applied a simple wet chemical method to deposit CeO_2 nanoparticles on ultrathin Co_3O_4 nanosheets with a thickness of 3 nm. The synergistic effect between CeO_2 and Co_3O_4, and the stable open 2D structure significantly reduced reaction temperature for the complete catalytic oxidation of CO. Sun *et al.* [92] first synthesized an ultrathin $CeCO_3OH$ sheet precursor by a solvothermal method, which was calcined to obtain a single-layer CeO_2 nanosheet with a thickness of only 0.6 nm. This single-layer CeO_2 contained a large number of pits, where the low-coordination Ce site was the center of catalytic oxidation. The four-coordinated Ce was responsible for the adsorption of CO, while the five-coordinated Ce promoted O_2 activation. The synergistic effect between these two types of Ce reduced the activation barrier. Compared with bulk CeO_2, pit-rich 2D CeO_2 significantly enhanced the catalytic oxidation of CO.

3.2. O_3

Although ozone (O_3) in the stratosphere can absorb ultraviolet to protect the ecological environment, O_3 in the troposphere (mainly coming from the photochemical reaction of VOCs and NO_x) is an important player in the formation of secondary VOCs and can cause respiratory and cardiovascular diseases [93]. Catalytic decomposition, an economical, safe and efficient method, can realize the fast conversion of O_3 to O_2 under ambient conditions, but also faces the challenges of high environmental humidity and high space velocity [94]. The first step in the catalytic decomposition of O_3 is the dissociation of O_3 into an O_2 molecule and an O atom [95]. Oxygen vacancies on the surface of low-cost TMOs are the active sites for O atoms and can also react with fresh O_3 to generate peroxide and superoxide species, whose desorption also forms O_2 molecules [96]. MnO_2 is the most concerning ozonolysis catalyst [97], and 2D ultrathin MnO_2 nanosheets expose

abundant oxygen vacancies. To prevent oxygen vacancies from being occupied by environmental H_2O molecules, Cao *et al.* [98] prepared oxygen vacancy-rich 2D δ-MnO_2 with a thickness of 2-3 nm through the adjustment of NH_4^+ concentration. The adsorption of NH_4^+ on [MnO_6] crystallites reduced the surface energy of [MnO_6] nanosheets, greatly promoting 2D growth. Moreover, the surface-adsorbed NH_4^+ promoted O_3 adsorption and abated the competitive adsorption of H_2O molecules. Furthermore, NH_4^+ accelerated the desorption of the peroxide species, which was a key intermediate (Fig. 3b). Therefore, 2D δ-MnO_2 maintained a 100% decomposition efficiency of 100 ppm O_3 over 36 h at 50% relative humidity and a high space velocity at 25 °C (Fig. S1b in Supporting information). Gopi *et al.* [99] applied HNO_3 to treat ultrathin δ-MnO_2 nanosheets so that interlayer K^+ was replaced by H^+ to obtain H-δ-MnO_2. This cation exchange promoted an increase in the specific surface area, pore volume, Mn^{3+} content, and surface oxygen vacancies. Therefore, the transportation, adsorption, and catalytic decomposition of O_3 were promoted. H-δ-MnO_2 achieved 100% removal efficiency of 200–3000 ppm O_3.

3.3. NO_x

Nitrogen oxides (NO_x, including NO and NO_2), originating from power stations, chemical plants, and transport emissions, are important culprits of air pollution, such as acid rain, ozonosphere destruction, photochemical pollution, and haze [100]. Selective catalytic reduction of NO_x with NH_3 (NH_3-SCR) is the most widely applied deNOx technology, which uses NH_3 to reduce NO and NO_2 into N_2 and H_2O under the action of catalysts [101]. However, the commercial vanadium-based oxides (V_2O_5/TiO_2 or V_2O_5-WO_3/TiO_2) still suffer poor low-temperature activity, weak resistance to sulfur/H_2O, and biological toxicity [102]. 2D TMOs have the potential to be green, economical, and efficient alternative catalysts. Heo *et al.* [103] supported 2D V_2O_5 nanoflakes (NF V_2O_5-W/T) with a thickness of 2-10 nm on WO_3/TiO_2 as a low-temperature catalyst for NH_3-SCR reduction of NO. Compared with the commercial catalyst V_2O_5-W/T, the V^{4+}/V^{5+} ratio of the 2D V_2O_5 nanoflakes was higher, prompting a shift of the temperature window to a lower temperature (100% deNOx conversion efficiency is achieved at 221 °C). Zheng *et al.* [104] reported a facile strategy to impregnate Mn species on 1.7 nm-thick 2D Co_3O_4 nanosheets to obtain Mn/Co_3O_4 catalysts, which realized a constant NO conversion rate above 80% between 175 and 300 °C and a high tolerance to H_2O (Fig. S1c in Supporting information). The ultrathin 2D nanosheet structure can facilitate the adsorption of gaseous reactants. The strong interaction between cobalt and manganese oxides accelerated the redox cycle and increased the amount of Co^{3+} and surface oxygen species, resulting in the enhanced NH_3-SCR activity. Surface acidity is one of the important factors determining the NH_3-SCR activity of TMOs. Ma *et al.* [105] prepared 2D CeO_2 nanosheets with a thickness of 1.7 nm. The surface of 2D CeO_2 possessed many pits, which could fully expose acid sites. Besides, MoO_x was introduced and highly dispersed on the surface of 2D nanosheet. The electron transfer between CeO_2 and MoO_x leads to the formation of undercoordinated Mo^{5+}, promoting the transformation of the Bronsted acid site to the more stable Lewis acid site at high temperature (Fig. 3c), and thereby increasing the catalytic activity.

3.4. Soot

Soot (mainly composed of nanocarbon particles), a major component in particles emitted by diesel engines, can harm the human respiratory system and cause severe haze [106]. The diesel particulate filter can effectively capture soot particles, but the temperature of diesel engine exhaust (200–400 °C) usually cannot meet the complete combustion temperature requirement of soot particles (~600 °C). Consequently, the accumulation of soot particles would cause a large exhaust pressure drop [107]. The currently concerned solid (reactant)-solid (catalyst)-gas (oxidant) catalytic system can effectively reduce the combustion temperature and convert soot into CO_2. Inexpensive TMOs with high redox capacity and excellent thermal stability are considered the most promising soot combustion catalysts [108]. In addition, 2D metal oxide-assembled nanosheets generate large macro porous voids, greatly increasing soot capture [109]. Li *et al.* [110] synthesized a series of Fe-doped porous ultrathin Co_3O_4 nanosheets by a one-pot MgO-mediated method. When Fe/Co was 1/4, the catalyst exhibited the highest soot oxidation catalytic performance (T90 = 351 °C). Furthermore, the study found that the 2D nanosheets provided a larger external surface area for the contact between the catalyst and soot, and the porous structure facilitated the adsorption and diffusion of reactive gases. In addition, Fe doping was favorable for the formation of oxygen vacancies and the adsorption of gaseous O_2, effectively improving the catalytic activity of soot oxidation (Fig. 3d). Similarly, Cui *et al.* [111] constructed Ce-doped Co_3O_4 nanosheets to utilize a porous 2D structure with a large specific surface area to promote the solid-solid contact of soot catalytic combustion at the three-phase interface. Moreover, Ce doping facilitated the formation of superoxide species and $O_2^{\delta-}$ species. Therefore, the catalytic performance of CoCe-HNS is superior than that of CeO_2 and Ce-doped Co_3O_4 nanosheets, as well as Co_3O_4 and Ce-doped Co_3O_4 nanoparticles (Fig. S1d in Supporting information). In addition to ROS, NO and soot are produced together in the exhaust gas of diesel engines, and NO can be converted into NO_2 by TMOs as an oxidant for soot combustion [112]. For this, Shi *et al.* [113] obtained ultrathin MnO_{2-x} nanosheet arrays with a thickness of 3 nm by *in situ* etching of the La layer from $LaMnO_3$. The low-coordinated Mn in 2D MnO_{2-x} notably enhanced the surface reducibility. Moreover, the coexisting NO and O_2 reacted to generate NO_2 species, which decreased the ignition temperature (200 °C) of the soot in close contact with the nanosheets.

3.5. VOCs

Volatile organic compounds (VOCs) can not only pollute the atmosphere directly and indirectly (as the crucial precursor of photochemical smog and haze), but also endanger human health [114]. Catalytic oxidation is one of the most effective and economically feasible technologies by oxidizing various VOCs into CO_2, H_2O and other relatively less harmful compounds at lower temperatures [115]. TMOs (especially Mn [116], Co [117], Ce [118], and Cu [119] based oxides) possess the advantages of low cost, excellent thermal stability, and good redox performance for VOC purification [120]. Surface high-valent metal sites, oxygen vacancies, and surface-active lattice oxygen are key reaction sites for VOC oxidation [121]. the amount of these reaction sites exposed could be substantially increased and exposed by constructing a 2D structure. In view of complex characteristics of VOCs, this section selects two typical polluting VOCs, benzene series (BTEX) and formaldehyde (HCHO), as the target pollutants for the introduction of VOCs oxidation over 2D TMOs.

Structurally stable BTEX is the common VOCs in industrial and indoor air with strong toxicity and can migrate over long distances to damage the atmospheric environment and human health [122,123]. MnO_2 is an important catalyst for BTEX oxidation. The redox properties of 2D MnO_2 can be easily controlled due to the replaceability of interlayer cations. Liu *et al.* [124] prepared 2D layered MnO_2 containing Ce^{3+} and Cu^{2+} between layers (named Ce-MnO_2 and Cu-MnO_2) for catalytic oxidation of benzene. Compared with pristine MnO_2, the catalytic activity of interlayer ion-replaced MnO_2 was significantly improved (Fig. S1e in Supporting informa-

tion). Especially, Cu-MnO_2 exhibits the highest reaction rate and excellent stability, which is attributed to best surface reducibility, the highest lattice oxygen reactivity, and the most oxygen vacancies. In addition, Cu^{2+} is beneficial to improving the surface hydrophobicity of MnO_2, enhancing the water poisoning resistance. To explore the effect of oxygen vacancies in 2D MnO_2, Dong *et al.* [125] used Cu^{2+} to replace the original interlayer K^+ of MnO_2 to induce Mn^{3+} formation, which could regulate the concentration of oxygen vacancies. This study found that a moderate content of oxygen vacancies was conducive to the low-temperature reducibility and the increased concentration of ROS, promoting the catalytic activity of Cu-MnO_2 (Fig. 3e). Wang *et al.* [126] developed a "redox-precipitation" synthesis scheme, where $CoMn_xO_y$ nanosheet catalysts with atomic dispersion were prepared by the reaction among Mn^{7+}, Co^{2+} and Mn^{2+}. The prepared $CoMn_xO_y$ with a large specific surface area was composed of 2 to 5 porous monolayers, where the Co_3O_4 phase was uniformly distributed in the $MnCo_2O_{4.5}$ phase and constituted the active Co_3O_4-$MnCo_2O_{4.5}$ interface. A large amount of oxygen vacancies were generated on this interface to dissociate O_2 into ROS, which participated in the oxidation of adsorbed toluene.

HCHO can cause serious health problems and even induce cancer as a major indoor gaseous pollutant [127,128]. Low-temperature catalytic oxidation is the most effective and harmless treatment technology so far and can completely mineralize HCHO into CO_2 and H_2O [129]. Currently, studies have been devoted to realizing the low-temperature or room-temperature catalytic oxidation of HCHO over 2D TMOs. Our group applied the solvothermal method to precisely control the thickness of Co_3O_4 nanosheets (from 2 to 20 nm), and investigated the effect of different thickness-induced changes in active site exposure on the reaction pathway of HCHO oxidation [130]. The results showed that the ultrathin Co_3O_4 nanosheets (Co_3O_4-2) with atomic layer thickness (~2 nm) exhibited stronger lattice disorder than the other three thicker nanosheets. Further, the 2D and disordered structure of Co_3O_4-2 enhanced the surface exposure of active sites (Co^{3+} and oxygen vacancies). Co_3O_4-2 can activate O_2 and H_2O to produce the most ROS, avoiding the generation of intermediate species that are difficult to desorb and decompose, which can occupy active sites and lead to the inhibition of HCHO oxidation. Therefore, Co_3O_4-2 achieved long-term purification of 1 ppm HCHO at room temperature (Fig. S1f in Supporting information). Alkali metal ion-modified TMOs have been proven to significantly improve the low-temperature HCHO oxidation compared with original TMOs [131]. The interlayers of 2D MnO_2 can accommodate alkali metal ions. Based on this, Wang *et al.* [132] fabricated ultrathin (< 2 nm) MnO_2 nanosheets with large lateral dimensions of Na^+, K^+, and Cs^+ intercalation by molten salt method. This study demonstrates that alkali metal ions can significantly reduce the oxygen vacancy formation energy of MnO_2 through charge balance. The Cs-intercalated MnO_2 with the most oxygen vacancies can achieve 90% conversion of 200 ppm HCHO at 65 °C. Mechanistic studies show that oxygen vacancies capture O_2 to form adsorbed ROS, which degrades the formate intermediate into CO_2 and H_2O (Fig. 3f).

4. Conclusion and outlook

In conclusion, this review summarizes and compares preparation methods of 2D TMOs including top-down and bottom-up preparation methods. The specific applications of 2D TMOs in the elimination of atmospheric inorganic pollutants and volatile organic pollutants are also expounded. Although great progress has been made in the fields pertaining to 2D TMOs, further research is still demanded on the optimization of the preparation method, the low-temperature activity improvement and practical applications.

(1) The current preparation methods of 2D TMOs still have great limitations. For most non-layered oxides, it is difficult to prepare single-layer or few-layer ultrathin nanosheets. In general, cumbersome procedures and additional reagents (potentially toxic and expensive) are required. Therefore, green, economical, and high-yield catalyst preparation is urgently needed. Organic or inorganic 2D structures of natural organisms often possess extraordinary properties or functions [133,134]. Therefore, biomimetic design incorporating nanomaterials may shed light on new preparation methods for high-performance 2D TMOs.
(2) The temperature required for the catalytic elimination of most atmospheric pollutants over 2D TMOs is relatively high, leading to large energy consumption and increased operating costs. Elucidating the relationship between 2D microstructure and reaction mechanism through high-precision *in situ* characterization is an important solution, which can provide guidance for the design of TMOs with more efficient 2D structure and address the key limiting barriers responsible for low-temperature activity.
(3) Most 2D transition metal oxides exhibit a powder form, limiting their application in purification devices. Therefore, the development of efficient and highly stable monolithic catalysts based on 2D metal oxide nanosheets is the key to practical applications of 2D TMOs. We believe that 2D MnO_x, an inexpensive and high-performance catalyst, is the most promising active component supported on metal foams or ceramics to obtain monolithic catalysts. Because the native layered structure of δ-MnO_2 facilitates its loading under low-temperature, simple reaction conditions.

Declaration of competing interest

The authors declare that they have no known competing financial interests or personal relationships that could have appeared to influence the work reported in this paper.

Acknowledgments

This work was supported by the Strategic Priority Research Program of the Chinese Academy of Sciences, China (Nos. XDA23010300 and XDA23010000), National Natural Science Foundation of China (Nos. 51878644 and 41573138), the National Key Research and Development Program of China (No. 2016YFA0203000), and the Plan for "National Youth Talents" of the Organization Department of the Central Committee.

Supplementary materials

Supplementary material associated with this article can be found, in the online version, at doi:10.1016/j.cclet.2022.108000.

References

[1] M. Li, H. Liu, G.N. Geng, et al., Natl. Sci. Rev. 4 (2017) 834–866.
[2] Z. Miao, T. Balezentis, S. Shao, et al., Energy Econ. 83 (2019) 501–514.
[3] K. Li, J.L. Li, S.R. Tong, et al., Atoms Chem. Phys. 19 (2019) 8021–8036.
[4] W.J. Guan, X.Y. Zheng, K.F. Chung, et al., Lancet 388 (2016) 1939–1951.
[5] M.E. Heroux, H.R. Anderson, R. Atkinson, et al., Int. J. Public Health 60 (2015) 619–627.
[6] H.B. Fu, J.M. Chen, Sci. Total Environ. 578 (2017) 121–138.
[7] M.X. Liu, X. Huang, Y. Song, et al., Proc. Natl. Acad. Sci. U. S. A. 116 (2019) 7760–7765.
[8] T. Wang, L.K. Xue, P. Brimblecombe, et al., Sci. Total. Environ. 575 (2017) 1582–1596.
[9] C.H.A. Tsang, K. Li, Y.X. Zeng, et al., Environ. Int. 125 (2019) 200–228.
[10] Y.Z. Liu, R.T. Guo, C.P. Duan, et al., Chemsphere 262 (2021) 127886.
[11] H.M. Xu, N.Q. Yan, Z. Qu, et al., Environ. Sci. Technol. 51 (2017) 8879–8892.
[12] Y. Shan, Y.X. Liu, Y. Li, et al., Sep. Purif. Technol. 250 (2020) 117181.
[13] C. Peng, D. Yu, L.Y. Wang, et al., J. Mater. Chem. A 9 (2021) 12947–12980.
[14] P. Wu, X.J. Jin, Y.C. Qiu, et al., Environ. Sci. Technol. 55 (2021) 4268–4286.

[15] S. Zhang, T. Hedtke, X.C. Zhou, et al., ACS EST Eng. 1 (2021) 706–724.
[16] Y.W. Zhang, J.S. Xu, J. Mei, et al., J. Hazard. Mater. 394 (2020) 122529.
[17] J. Mei, T. Liao, Z.Q. Sun, Energy Environ. Mater. 5 (2022) 115–132.
[18] J. Bae, D. Shin, H. Jeong, et al., ACS Catal. 11 (2021) 11066–11074.
[19] Z.Y. Wu, T. Liao, S. Wang, et al., Nano Micro Lett. 14 (2022) 90.
[20] Z.Y. Wu, J. Mei, Q. Liu, et al., J. Mater. Chem. A 10 (2022) 808–817.
[21] G. Chen, Y. Cai, H. Zhang, et al., Environ. Sci. Technol. 55 (2021) 14204–14214.
[22] Y.Q. Guo, K. Xu, C.Z. Wu, et al., Chem. Soc. Rev. 44 (2015) 637–646.
[23] Y. Dou, L. Zhang, X. Xu, et al., Chem. Soc. Rev. 46 (2017) 7338–7373.
[24] P. Kumbhakar, C.C. Gowda, P.L. Mahapatra, et al., Mater. Today 45 (2021) 142–168.
[25] J.L. Wang, G.K. Zhang, P.Y. Zhang, et al., J. Mater. Chem. A 5 (2017) 5719–5725.
[26] Y. Li, F.M. Li, X.Y. Meng, et al., ACS Catal. 8 (2018) 1913–1920.
[27] T. Yang, T.T. Song, M. Callsen, et al., Adv. Mater. Interfaces 6 (2019) 1801160.
[28] J. Mei, T. Liao, Z.Q. Sun, J. Energy Chem. 27 (2018) 117–127.
[29] J. Mei, J. Shang, T.W. He, et al., Adv. Energy Mater. 12 (2022) 2201141.
[30] J. Mei, T.W. He, J. Bai, et al., Adv. Mater. 33 (2021) 2104638.
[31] C. Tan, H. Zhang, Nat. Commun. 6 (2015) 7873.
[32] K. Kalantar-zadeh, J.Z. Ou, T. Daeneke, et al., Appl. Mater. Today 5 (2016) 73–89.
[33] M. Shamoto, T. Tanimoto, K. Tomono, et al., Electr. Trans. 50 (2013) 85–92.
[34] Z. Xiao, J. Meng, F. Xia, et al., Energy Environ. Sci. 13 (2020) 3129–3137.
[35] P. Xiong, R. Ma, N. Sakai, et al., ACS Appl. Mater. Interfaces 9 (2017) 6282–6291.
[36] H.G. Xie, Z. Li, L. Cheng, et al., iScience 25 (2022) 103598.
[37] P. Tao, S. Yao, F. Liu, et al., J. Mater. Chem. A 7 (2019) 23512–23536.
[38] H. Shin, J. Ahn, D.H. Kim, et al., MRS Bull. 46 (2021) 1080–1094.
[39] V.S. Bhati, M. Kumar, R. Banerjee, J. Mater. Chem. C 9 (2021) 8776–8808.
[40] P. Xiong, R.Z. Ma, G.X. Wang, et al., Energy Storage Mater. 19 (2019) 281–298.
[41] N. Mahmood, I.A. De Castro, K. Pramoda, et al., Energy Storage Mater. 16 (2019) 455–480.
[42] H. Miao, Z. Teng, C. Wang, H, et al., Chem. Eur. J. 25 (2019) 929–944.
[43] L. Mei, S. Zhu, W. Yin, et al., Theranostics 10 (2020) 757–781.
[44] B. Ren, Y. Wang, J.Z. Ou, J. Mater. Chem. B 8 (2020) 1108–1127.
[45] J. Mei, T. Liao, L.Z. Kou, et al., Adv. Mater. 29 (2017) 1700176.
[46] Z. Sun, T. Liao, L. Kou, Sci. China Mater. 60 (2017) 1–24.
[47] A. Raza, J.Z. Hassan, M. Ikram, et al., Adv. Mater. Interfaces 8 (2021) 2002205.
[48] M.M.Y.A. Alsaif, M.R. Field, T. Daeneke, et al., ACS Appl. Mater. Interfaces 8 (2016) 3482–3493.
[49] D. Hanlon, C. Backes, T.M. Higgins, et al., Chem. Mater. 26 (2014) 1751–1763.
[50] G. Cunningham, M. Lotya, C.S. Cucinotta, et al., ACS Nano 6 (2012) 3468–3480.
[51] A. Gupta, S. Vasudevan, J. Phys. Chem. C 122 (2018) 19243–19250.
[52] R.Z. Ma, T. Sasaki, Acc. Chem. Res. 48 (2015) 136–143.
[53] T. Taniguchi, L. Nurdiwijayanto, R.Z. Ma, et al., Appl. Phys. Rev. 9 (2022) 021313.
[54] F. Geng, R. Ma, Y. Ebina, et al., J. Am. Chem. Soc. 136 (2014) 5491–5500.
[55] R. Ma, T. Sasaki, Acc. Chem. Res. 48 (2015) 136–143.
[56] J.M. Lee, B. Kang, Y.K. Jo, et al., ACS Appl. Mater. Interfaces 11 (2019) 12121–12132.
[57] S. Yang, P.P. Zhang, A.S. Nia, et al., Adv. Mater. 32 (2020) 1907857.
[58] Z. Kou, K. Wang, Z. Liu, et al., Small Struct. 3 (2022) 2100153.
[59] Y. Yang, X. Qiu, W. Shi, et al., Chem. Eng. J. 408 (2021) 127247.
[60] L.S. Yang, W.J. Chen, Q.M. Yu, et al., Nano Res. 14 (2021) 1583–1597.
[61] Y. Jia, X. Yi, Z. Li, et al., Talanta 219 (2020) 121308.
[62] H.R. Rasouli, J. Kim, N. Mehmood, et al., Nano Lett. 21 (2021) 3997–4005.
[63] L. Li, F. Lu, W. Xiong, et al., Natl. Sci. Rev. 9 (2022) 153.
[64] L. Miao, X. Tang, S. Zhao, et al., Nano. Res. 15 (2022) 1660–1671.
[65] W. Li, D. Liu, X. Feng, et al., Adv. Energy Mater. 9 (2019) 1803583.
[66] J.F. Li, G.Z. Lu, Y.Q. Wang, et al., J. Colloid. Inter. Sci. 377 (2012) 191–196.
[67] X. Liu, Y. Sun, M. Yu, et al., Sens. Actuator B Chem. 255 (2018) 3384–3390.
[68] H. Yu, Q. Liao, Z. Kang, et al., Small 16 (2020) 2005520.
[69] Y.Q. Jiang, L.Y. Chen, H.Q. Zhang, et al., Chem. Eng. J. 292 (2016) 1–12.
[70] S. Gao, Z. Sun, W. Liu, et al., Nat. Commun. 8 (2017) 14503.
[71] X. Wang, K. Klingan, M. Klingenhof, et al., Nat. Commun. 12 (2021) 794.
[72] Y. Zhao, C. Chang, F. Teng, et al., Adv. Energy. Mater. 7 (2017) 1700005.
[73] Z. Sun, T. Liao, Y. Dou, et al., Nat. Commun. 5 (2014) 3813.
[74] J. Zhang, X. Lin, D. Xue, et al., Nanoscale 11 (2019) 3200–3207.
[75] M. Xing, A. Gao, Y. Liang, et al., ACS Appl. Energy Mater. 4 (2021) 888–898.
[76] T.J. Liu, J.W. Ding, Z.Q. Su, et al., Mater. Today Eng. 6 (2017) 79–95.
[77] H.L. Cao, X.F. Zhou, C. Zheng, et al., ACS Appl. Mater. Interfaces 7 (2015) 11984–11990.
[78] H.W. Zhao, Y.J. Zhu, F.S. Li, et al., Angew. Chem. Int. Ed. 56 (2017) 8766–8770.
[79] L. Lei, Z. Wu, H. Liu, et al., J. Mater. Chem. A 6 (2018) 9948–9961.
[80] W. Eom, A. Kim, H. Park, et al., Adv. Funct. Mater. 26 (2016) 7605–7613.
[81] X. Xiao, H. Song, S. Lin, et al., Nat. Commun. 7 (2016) 11296.
[82] Y. Li, W. Yang, Z. Tu, et al., J. Alloy. Compd. 857 (2021) 157626.
[83] S.K. Gupta, Y. Mao, Procedia Mater. Sci. 117 (2021) 100734.
[84] Z. Hu, X. Xiao, H. Jin, et al., Nat. Commun. 8 (2017) 15630.
[85] J. Gu, C. Zhang, Z. Du, et al., Small 15 (2019) 1904587.
[86] S. Dey, G.C. Dhal, Aerosol Sci. Eng. 3 (2019) 97–131.
[87] J.J. Rose, L. Wang, Q. Xu, et al., Am. J. Respir. Crit. Care 195 (2017) 596–606.
[88] S. Royer, D. Duprez, ChemCatChem 3 (2011) 24–65.
[89] J. Bae, D. Shin, H. Jeong, et al., ACS Catal. 9 (2019) 10093–10100.
[90] Y. Cai, J. Xu, Y. Guo, et al., ACS Catal. 9 (2019) 2558–2567.
[91] X. Jin, Y. Duan, D. Liu, et al., ACS Appl. Nano. Mater. 2 (2019) 5769–5778.
[92] Y. Sun, Q. Liu, S. Gao, et al., Nat. Commun. 4 (2013) 2899.
[93] H. Lu, X. Lyu, H. Cheng, et al., Environ. Sci. Process. Impacts 21 (2019) 916–929.
[94] X.T. Li, J.Z. Ma, H. He, J. Environ. Sci. 94 (2020) 14–31.
[95] Y.X. Yu, H.N. Wang, H. Li, et al., Chemsphere 298 (2022) 134187.
[96] G. Zhu, J. Zhu, W. Jiang, et al., Appl. Catal. B: Environ. 209 (2017) 729–737.
[97] L. Zhang, S. Wang, L. Lv, et al., Langmuir 37 (2021) 1410–1419.
[98] R. Cao, L. Li, P. Zhang, et al., Environ. Sci. Nano 8 (2021) 1628–1641.
[99] T. Gopi, G. Swetha, S.C. Shekar, et al., Catal. Commun. 92 (2017) 51–55.
[100] Y. Liu, J. Zhao, J.M. Lee, ChemCatChem 10 (2018) 1499–1511.
[101] J. Xu, G. Chen, F. Guo, et al., Chem. Eng. J. 353 (2018) 507–518.
[102] F. Gao, X. Tang, Z. Sani, et al., Catal. Sci. Technol. 10 (2020) 7486–7501.
[103] J.G. Heo, M. Ullah, M.P. Chun, et al., Inorg. Chem. Commun. 137 (2022) 109191.
[104] K. Zheng, Z. Zhou, Y. Wang, et al., Catal. Sci. Technol. 10 (2020) 3450–3457.
[105] N. Ma, Z. Hao, G. Liu, et al., J. Environ. Chem. Eng. 10 (2022) 108114.
[106] H.A. Michelsen, Proc. Combust. Inst. 36 (2017) 717–735.
[107] X. Zhao, J. E, G. Liao, F. Zhang, J. Chen, Y. Deng, et al., Fuel 290 (2021) 119795.
[108] R.P. Neha, S.V. Singh, J. Environ. Chem. Eng. 8 (2020) 103945.
[109] L. Xing, Y. Yang, C. Cao, et al., ACS Sustain. Chem. Eng. 6 (2018) 16544–16554.
[110] Y. Li, K. Li, Y. Wang, et al., Chem. Eng. J. 431 (2022) 133248.
[111] B. Cui, L. Zhou, K. Li, et al., Appl. Catal. B: Environ. 267 (2020) 118670.
[112] C. Cao, L. Xing, Y. Yang, et al., Appl. Surf. Sci. 406 (2017) 245–253.
[113] Q. Shi, T. Liu, Q. Li, et al., Appl. Catal. B: Environ. 246 (2019) 312–321.
[114] N.M. Hanif, N.S.S.L. Hawari, M. Othman, et al., Chemsphere 285 (2021) 131355.
[115] C. He, J. Cheng, X. Zhang, et al., Chem. Rev. 119 (2019) 4471–4568.
[116] W. Yang, Z.A. Su, Z. Xu, et al., Appl. Catal. B: Environ. 260 (2020) 118150.
[117] J. Zhong, Y. Zeng, D. Chen, et al., J. Hazard. Mater. 386 (2020) 125375.
[118] Y. Zeng, K.G. Haw, Z. Wang, et al., J. Hazard. Mater. 404 (2021) 124088.
[119] Q. Li, N. Luo, D. Xia, et al., Environ. Sci. Nano 9 (2022) 781–796.
[120] Y. Guo, M. Wen, G. Li, et al., Appl. Catal. B: Environ. 281 (2021) 119447.
[121] H. Huang, Y. Xu, Q. Feng, et al., Catal. Sci. Technol. 5 (2015) 2649–2669.
[122] B. Yu, Z. Yuan, Z. Yu, et al., Chem. Eng. J. 435 (2022) 134825.
[123] P. Lucialli, S. Marinello, E. Pollini, et al., Atom. Pollut. Res. 11 (2020) 1998–2010.
[124] Y. Liu, W. Zong, H. Zhou, et al., Catal. Sci. Technol. 8 (2018) 5344–5358.
[125] C. Dong, Z. Qu, X. Jiang, et al., J. Hazard. Mater. 391 (2020) 122181.
[126] Y. Wang, L. Guo, M. Chen, et al., Catal. Sci. Technol. 8 (2018) 459–471.
[127] T. Salthammer, Angew. Chem. Int. Ed. 52 (2013) 3320–3327.
[128] T. Salthammer, Build. Environ. 150 (2019) 219–232.
[129] J. Ye, Y. Yu, J. Fan, et al., Environ. Sci. Nano 7 (2020) 3655–3709.
[130] R. Li, X. Shi, Y. Huang, et al., Appl. Catal. B: Environ. 319 (2022) 121902.
[131] Y. Li, X. Chen, C. Wang, et al., ACS Catal. 8 (2018) 11377–11385.
[132] Y. Wang, K. Liu, J. Wu, et al., ACS Catal. 10 (2020) 10021–10031.
[133] J. Mei, T. Liao, H. Peng, et al., Small Methods 6 (2022) 2101076.
[134] B. Wijerathne, T. Liao, K. Ostrikov, et al., Small Struct. 3 (2022) 2100228.